



UNIVERSITY OF LEEDS

This is a repository copy of *Linear Dynamics Modelling of Droplet Deformation in a Pulsatile Electric Field*.

White Rose Research Online URL for this paper:
<http://eprints.whiterose.ac.uk/104276/>

Version: Accepted Version

Article:

Vivacqua, V, Ghadiri, M orcid.org/0000-0003-0479-2845, Abdullah, AM et al. (5 more authors) (2016) Linear Dynamics Modelling of Droplet Deformation in a Pulsatile Electric Field. *Chemical Engineering Research and Design*, 114. pp. 162-170. ISSN 0263-8762

<https://doi.org/10.1016/j.cherd.2016.08.015>

© 2016, Elsevier. Licensed under the Creative Commons Attribution-NonCommercial-NoDerivatives 4.0 International
<http://creativecommons.org/licenses/by-nc-nd/4.0/>

Reuse

Unless indicated otherwise, fulltext items are protected by copyright with all rights reserved. The copyright exception in section 29 of the Copyright, Designs and Patents Act 1988 allows the making of a single copy solely for the purpose of non-commercial research or private study within the limits of fair dealing. The publisher or other rights-holder may allow further reproduction and re-use of this version - refer to the White Rose Research Online record for this item. Where records identify the publisher as the copyright holder, users can verify any specific terms of use on the publisher's website.

Takedown

If you consider content in White Rose Research Online to be in breach of UK law, please notify us by emailing eprints@whiterose.ac.uk including the URL of the record and the reason for the withdrawal request.



eprints@whiterose.ac.uk
<https://eprints.whiterose.ac.uk/>

Linear Dynamics Modelling of Droplet Deformation in a Pulsatile Electric Field

Vincenzino Vivacqua^{a, b}, Mojtaba Ghadiri^{b*}, Aboubakr M. Abdullah^a, Ali Hassanpour^b, Mohammed J. Al-Marri^c, Barry Azzopardi^d, Buddhika Hewakandamby^d, Bijan Kermani^e

^a Center for Advanced Materials, Qatar University, Doha 2713, Qatar

^b Institute of Particle Science and Engineering, University of Leeds, Leeds LS2 9JT, UK

^c Gas Processing Center, Qatar University, Doha 2713, Qatar

^d Department of Chemical and Environmental Engineering, University of Nottingham, Nottingham NG7 2RD, UK

^e Keytech, Camberley GU15 2BN, UK

Abstract

A linear dynamic model of water droplet deformation in the presence of an electric field has been developed. Analytical solutions of the differential equation of motion are provided with different waveforms as forcing terms, namely in the case of half-sinusoidal, square and sawtooth waves. The main dimensionless groups are identified as a result of this analysis. The predictions of the model are compared with some data of droplet deformation available in the literature. The calculations based on this model show that the waveform affects the response of the droplet to the electric field stimulus. Resonance is possible only when the droplets are sufficiently large (i.e. for Ohnesorge number less than 1). The oscillation amplitude decreases rapidly with the electric field frequency. A qualitative comparison with some experiments of droplet-interface coalescence available in the literature has also been addressed, suggesting a correlation between the formation of secondary droplets and the amplitude of oscillation of the mother droplet. The outcomes of this analysis can be useful for the selection of the best operating conditions to improve the electrocoalescence process efficiency, as they can provide guidelines to the choice of the most suitable electric field parameters.

Keywords: Electrocoalescence; Partial coalescence; Modelling; Water-in-oil emulsions; Phase separation.

*Corresponding author. Tel.: +44 113 343 2406; Fax: +44 113 343 2384.

E-mail address: m.ghadiri@leeds.ac.uk

1. Introduction

The application of an external electric field has been used in the petroleum industry to promote water droplet coalescence and facilitate separation of water-in-oil emulsions for many decades (Mhatre *et al.*, 2015). The presence of an externally applied electric field increases the rate of drainage of the oil film between two coalescing droplets (Mhatre *et al.*, 2015). However, incomplete coalescence can occur when the field strength is excessively high (Mousavi *et al.*, 2014; Mousavichoubeh *et al.*, 2011a; 2011b). Also, Taylor cones can form, causing electro-spraying (atomisation) of water droplets. The production of small progeny droplets adversely affects the separation efficiency as the removal of the water phase from the oil becomes more difficult. It would therefore be highly beneficial to know the operating conditions under which the onset of partial coalescence or atomisation is prevented. In this regard, Mousavichoubeh *et al.* (2011a) have shown that the formation of secondary droplets can be correlated with a dimensionless number, which is the product of the Weber and Ohnesorge numbers. In the light of their observation, they concluded that the phenomenon of partial coalescence is the result of two simultaneous actions: (i) pumping, driven by capillary pressure and resisted by the viscous drag, and (ii) the deformation and break-up due to the electrostatic pressure induced on the droplets by the application of the electric field. The electric field type also affects the pattern of coalescence, with the application of pulsed DC fields being beneficial to the enhancement of the process efficiency (Bailes and Larkai, 1981, Mousavi *et al.*, 2014; Vivacqua *et al.*, 2015). With respect to the mitigation of incomplete coalescence, Mousavi *et al.* (2014) report that the volume of the secondary droplets formed in the process decreases if pulse DC fields are employed, instead of constant fields. The electric field waveform and frequency also cause differences in behaviour. Mousavi *et al.* (2014), applied square, sawtooth and half-sinusoidal waves and obtained practically total suppression of partial coalescence with an applied field frequency in the range 1-100 Hz for the range of droplet size studied. Also, they showed that the half-sinusoidal and sawtooth waves are more effective in suppressing partial coalescence than the square waves.

The findings described above can have an important impact on the development of electrocoalescers. However, to define the optimum operational window for the properties of the liquids under consideration and the electric field configuration, it is necessary to analyse the phenomenon with a mathematical description of the electrocoalescence process. The functional dependence of the process performance on the wave type and frequency suggests that the analysis of the droplet dynamics is crucial for the description of the phenomenon, as the electrostatically-induced deformation is responsible for the occurrence of partial coalescence. The deformation of

single liquid droplets in another immiscible liquid under the application of an electric field has previously been studied extensively, as detailed below. The classical analytical theory of Taylor (1966), valid for small quasi-static deformations and constant fields, was extended later to AC fields by Torza *et al.* (1971). Subsequent studies were aimed at modifying the basic Taylor's electrohydrodynamic theory in order to address the discrepancies between experiments and model predictions (Ajayi, 1978; Baygents and Saville, 1989; Feng and Scott, 1996). In these studies, the original Taylor's approach was extended in order to obtain a complete and accurate theoretical description of the behavior of electrified water droplets. A more simplified approach has recently been undertaken by Gong *et al.* (2015) and Yan *et al.* (2015), where non-linear dynamic models of droplets deformation were developed to describe droplet deformation in the presence of time-varying fields. Gong *et al.* (2015) predict resonance frequencies for a 2 mm water droplet in sunflower oil under pulsed square fields. They suggested that the resonance frequencies represent the optimum frequency values in terms of efficiency for electrostatic demulsification. However, the existence of resonance for much smaller droplets, which are usually present in practical applications, was not discussed. Yan *et al.* (2015) applied their model for the prediction of water droplet oscillations in oil under AC and DC electric fields before Taylor cone break-up, with some level of disagreement between model predictions and experiments. For their analysis, a non-linear model was necessary to describe the droplet shape variation at high deformation. The transient oscillations of droplet deformation and breakup in the creeping flow under the presence of an electric field was theoretically studied by Sherwood (1988). He concluded that different modes of breakup are possible depending on the physical properties of the two fluids. According to the theoretical analysis of Basaran *et al.* (1995) the droplet would oscillate under small field strength, whereas at large field strengths, they do not oscillate any more but become unstable and issue jets of tiny droplets from their tips. Yeo *et al.* (2004) showed a pendant drop can exhibit resonance under AC electric field and droplets are ejected from the resonating meniscus.

The above-mentioned modelling attempts have not provided any indication of the selection of the most suitable electric field parameters for the optimisation of the process efficiency. For instance, no justification for the adoption of kHz frequencies in most available commercial electrocoalescers (Mhatre *et al.*, 2015) has been provided. In this paper, a linear model of droplet dynamics is applied to the case where a droplet is deforming under a pulsatile electric field. The effect of frequency and waveform is assessed by solving analytically the equation of motion of the droplet under the application of an electric field. The governing dimensionless group have been identified and the model predictions are compared with the behaviour observed in the literature.

2. Model

A linear model for droplet deformation under pulsatile electric fields is developed in this section. The model is based on a number of assumptions which are listed as follows: (i) the dynamic behaviour is described at small droplet deformation; (ii) the electrostatic pressure induced in the droplet is proportional to the square of the electric field intensity; (iii) the viscous damping is proportional to the velocity of deformation; (iv) gravity and buoyancy fully counteract each other and the added mass effect is neglected; (v) the water permittivity is much higher than that of the oil and both are independent of frequency; (vi) the interfacial tension is constant and independent of deformation; (vii) the dynamics of charge relaxation is neglected; (viii) the hydrodynamic and surface tension stresses based on the Torza et al. (1971)'s solution under sinusoidal waves are linearized and assumed to be approximately valid with a generic waveform. The effect of the waveform is considered in the electrostatic stress expression.

With reference to Figure 1a, we define a dimensionless displacement and a reduced time as:

$$\delta = \frac{\Delta r}{R} \quad (1)$$

$$\tau = t\omega_E \quad (2)$$

where ω_E is the frequency of the applied electric field. The stresses acting on the surface of the deformed droplet are illustrated in Figure 1b. The normal component of the electric stress is provided by Torza (1971) for a sinusoidal electric waveform. In the direction parallel to the field and considering the water as a perfect conductor, it reduces to (Yan *et al.*, 2015):

$$\sigma_E = \frac{9}{4} \varepsilon E_0^2 (1 - \cos 2\omega t) = \frac{9}{4} \varepsilon E_0^2 \sin^2 \omega t \quad (3)$$

It is now assumed that the effect of the electric field for a generic waveform can be captured by expressing the electric stress as:

$$\sigma_E = \frac{9}{4} \varepsilon E_0^2 \hat{E}^2 \quad (4)$$

where \hat{E} is the normalized waveform, E_0 is the peak value of the field strength.

During deformation, the droplet experiences a resistance to flow due to the hydrodynamic stresses at the droplet surface. Yan *et al.* (2015) simplified Torza's solution under the assumptions listed above. Using Eqs 1 and 2, the resulting equation can be rewritten as:

$$\sigma_{\mu} = -2\Lambda\mu\delta' \quad (5)$$

$$\Lambda = \frac{(19\lambda + 16)(2\lambda + 3)}{20(\lambda + 1)} \quad (6)$$

where λ is the ratio between the viscosity of the water and oil, and μ is the oil viscosity.

Yan *et al.* (2015) also provided the following equation for the difference in capillary pressure resulting:

$$\sigma_{\gamma} = \frac{2\gamma}{R} - \frac{\gamma}{R} \frac{8(1 + \delta) - 6}{(1 + \delta)^2} \quad (7)$$

As the purpose of this study is to describe the phenomenon at small deformations, a first order approximation of the previous expression will be used:

$$\sigma_{\gamma 0} = \sigma_{\gamma}|_{\delta=0} + \sigma'_{\gamma}|_{\delta=0} \delta = -\frac{4\gamma}{R} \delta \quad (8)$$

We shall now carry out a simplified force balance on the whole droplet. The force due to surface tension and electric field can be calculated multiplying the difference in capillary and electrostatic pressure by the drop cross sectional area (πR^2) while the viscous stress, assumed to be constant, will be multiplied by the drop external surface ($4\pi R^2$). Newton's second law of motion is then applied to obtain:

$$\frac{4}{3}\pi R^4 \rho \omega_E^2 \delta'' = -8\Lambda\mu\pi R^2 \omega_E \delta' - 4\pi R \gamma \omega_E \delta + \frac{9}{4}\pi R^2 \varepsilon E_0^2 \hat{E}^2 \quad (9)$$

whereas Yan *et al.* (2015) used the coefficient of the second derivative as an adjustable parameter.

Eq. 9 can also be rewritten as:

$$\delta'' + \frac{6\Lambda}{Re} \delta' + \frac{3}{We} \delta = \frac{27}{16Fr} \hat{E}^2 \quad (10)$$

where $Re = \rho R^2 \omega_E / \mu$, $We = \rho R^3 \omega_E^2 / \gamma$ and $Fr = \rho R^2 \omega_E^2 / (\varepsilon E_0^2)$ are the Reynolds, Weber and electrical Froude number, respectively. From Eq. 10, it is straightforward to obtain the steady state deformation, δ_{ss} , when a constant electric field is applied ($\hat{E} = 1$):

$$\delta_{ss} = \frac{9}{16} \frac{We}{Fr} = \frac{9}{16} We_{el} \quad (11)$$

where $We_{el} = R\varepsilon E_0^2 / \gamma$ is the electrical Weber number. According to Eq. 11, the deformation is proportional to the We_{el} number, in agreement with Taylor's analysis according to which a linear dependence is obtained at very small deformations. It is now possible to define a new normalized instantaneous deformation, $\bar{\delta}$, as:

$$\bar{\delta} = \frac{\delta}{\delta_{ss}} \quad (12)$$

Eq. 10 can now be expressed as Eq. 13:

$$\bar{\delta}'' + \frac{6\Lambda}{Re} \bar{\delta}' + \frac{3}{We} \bar{\delta} = \frac{3}{We} \hat{E}^2 \quad (13)$$

It is interesting to observe that Eq. 13 is mathematically equivalent to the equation of motion of a damped harmonic oscillator with a forcing term:

$$\bar{\delta}'' + 2\zeta\omega_n\bar{\delta}' + \omega_n^2\bar{\delta} = \omega_n^2\hat{E}^2 \quad (14)$$

with a dimensionless natural frequency ω_n and damping ratio ζ equal to:

$$\omega_n = \sqrt{\frac{3}{We}} \quad (15)$$

$$\zeta = \Lambda \frac{\sqrt{3We}}{Re} = \Lambda\sqrt{3} Oh \quad (16)$$

where $Oh = \mu/\sqrt{\rho\gamma R}$ is the Ohnesorge number. Equation 14 can be solved analytically with the initial conditions:

$$\delta|_{\tau=0} = \delta'|_{\tau=0} = 0 \quad (17)$$

The basic steps for obtaining a solution through Laplace transformation are as follows. The transform of Eq.14 with the initial conditions given by Eqs 17 provides an algebraic expression in the Laplace domain:

$$\bar{\delta}(s) = \omega_n^2 \frac{\hat{E}^2(s)}{s^2 + 2\zeta\omega_n s + \omega_n^2} \quad (18)$$

The s-transform of $\hat{E}^2(s)$ for one period depends on the waveform as given in Table 1. For periodic functions the transform of the forcing function can be calculated from Eq. 19:

$$\hat{E}^2(s) = \frac{1}{(1 - e^{-s})} \int_0^1 e^{-s\tau} \hat{E}_1^2(\tau) d\tau \quad (19)$$

where $\hat{E}_1(\tau)$ is the time function of the dimensionless electric field in one period.

After substitution of Eq. 19 into Eq. 18, the solution in the time domain can be obtain by applying the well-known technique of decomposition into partial fractions with the exponential terms becoming step functions in the time domain.

The algebraic equation describing droplet deformation will now be derived for different waveforms, namely for half-sinusoidal, square and sawtooth waves applied as forcing functions. These solutions will be given in terms of ζ and ω_n , so that, as far as a linear model can be applied, the results are valid independently of the accuracy of the numerical coefficients in the force terms.

2.1 Half- Sinusoidal waves

This type of waveform can be expressed mathematically as:

$$\hat{E} = |\sin(\pi\tau)| \quad (20)$$

The solution of Eq. 14 for a half-sinusoidal electric field input is for $\zeta < 1$:

$$\bar{\delta}_{sin} = \frac{1}{2} \{1 - [K_1 \cos(2\pi\tau) + K_2 \sin(2\pi\tau)]\} + e^{-\zeta\omega_n\tau} \left[K_3 \cos(\omega_0\tau) + K_4 \zeta \frac{\omega_n}{\omega_0} \sin(\omega_0\tau) \right] \quad (21)$$

whereas for $\zeta > 1$:

$$\bar{\delta}_{sin} = \frac{1}{2} \{1 - [K_1 \cos(2\pi\tau) + K_2 \sin(2\pi\tau)]\} + e^{-\zeta\omega_n\tau} \left[K_3 \cosh(\omega_0\tau) + K_4 \zeta \frac{\omega_n}{\omega_0} \sinh(\omega_0\tau) \right] \quad (22)$$

where:

$$\omega_0 = \omega_n \sqrt{|\zeta^2 - 1|} = \frac{3}{2} \sqrt{\frac{|Oh^2 - 1/3|}{We}} \quad (23)$$

It is noteworthy that Eqs 21 and 22 are formally identical, apart from the substitution of trigonometric functions by their respective hyperbolic functions. Hyperbolic functions have been used to highlight the similarity of the solutions; however, simplification of the exponential terms can be more convenient for numerical evaluation of the response, in order to avoid the computation of very large number associated with the hyperbolic operations.

The constants in Eqs 21 and 22 are calculated by the following relationships:

$$K_1 = \frac{\omega_n^2 [\omega_n^2 - (2\pi)^2]}{[\omega_n^2 - (2\pi)^2]^2 + (4\pi\omega_n\zeta)^2} \quad (24)$$

$$K_2 = \frac{4\pi\zeta\omega_n^3}{[\omega_n^2 - (2\pi)^2]^2 + (4\pi\omega_n\zeta)^2} \quad (25)$$

$$K_3 = \frac{2\pi^2 [\omega_n^2 - 4\zeta^2\omega_n^2 - (2\pi)^2]}{[\omega_n^2 - (2\pi)^2]^2 + (4\pi\omega_n\zeta)^2} \quad (26)$$

$$K_4 = \frac{2\pi^2 [\omega_n^2 - 4\zeta^2\omega_n^2 - (2\pi)^2]}{[\omega_n^2 - (2\pi)^2]^2 + (4\pi\omega_n\zeta)^2} \quad (27)$$

After a sufficiently long time, the exponential terms in Eqs 21 and 22 can be neglected and the amplitude of the response can be calculated as:

$$A = \frac{\omega_n^2}{\sqrt{[\omega_n^2 - (2\pi)^2]^2 + (4\pi\omega_n\zeta)^2}} \quad (28)$$

2.2 Square waves

Pulsed square waves can be defined as:

$$\hat{E} = \begin{cases} 1 & k \leq \tau \leq k + 1/2 \\ 0 & k + 1/2 < \tau \leq k + 1 \end{cases} \quad k = 0, 1, 2 \dots \quad (29)$$

The solution of Eq. 14 can be expressed as a combination of Heaviside functions and the response to a unit step change in the electric fields. For a step change ($\hat{E} = 1$), the dynamic response in terms of droplet deformation is given by:

$$\bar{\delta}_{step} = 1 - e^{-\zeta\omega_n\tau} \left[\cos(\omega_0\tau) + \zeta \frac{\omega_n}{\omega_0} \sin(\omega_0\tau) \right] \quad (30)$$

for the underdamped case ($\zeta < 1$), whereas for the overdamped case ($\zeta > 1$) we have:

$$\bar{\delta}_{step} = 1 - e^{-\zeta\omega_n\tau} \left[\cosh(\omega_0\tau) + \zeta \frac{\omega_n}{\omega_0} \sinh(\omega_0\tau) \right] \quad (31)$$

The solution for pulsed square waves can be formulated making use of the previous results as:

$$\bar{\delta}_{square} = \sum_{n=0}^{\infty} \theta(\tau - n) \bar{\delta}_{step}(\tau - n) - \theta(\tau - n - 0.5) \bar{\delta}_{step}(\tau - n - 0.5) \quad (32)$$

where $\theta(\tau - n)$ and $\theta(\tau - n - 0.5)$ are the Heaviside functions; the step change occurs at $\tau = n$ and $\tau = n + 0.5$, respectively. It should be noted that the parenthesis following the response to a step change in the electric field denotes a substitution of the time variable (e.g. τ is replaced by $\tau - n$ in the first term of Eq. (31) when evaluating $\bar{\delta}_{step}$). For the sake of a simpler notation, we will consider that the Heaviside function also brings about this variable substitution, i.e. Eq. 32 can be rewritten as:

$$\bar{\delta}_{square} = \sum_{n=0}^{\infty} \theta(\tau - n) \bar{\delta}_{step} - \theta(\tau - n - 0.5) \bar{\delta}_{step} \quad (33)$$

2.3 Sawtooth waves

The sawtooth wave can be defined as:

$$\hat{E} = \begin{cases} \tau & 0 \leq \tau \leq 1 \\ \hat{E}(\tau) = \hat{E}(\tau - 1) & \tau > 1 \end{cases} \quad (34)$$

The solution of Eq. 14 considering sawtooth waves can be obtained by superimposing the effect of simpler forcing functions. For an underdamped system ($\zeta < 1$), a quadratic change in the electric field ($\hat{E}^2 = \tau^2$) and a ramp input ($\hat{E}^2 = \tau$) bring about the following responses, respectively:

$$\bar{\delta}_{quad} = \frac{1}{2}\tau^2 - 2\frac{\zeta}{\omega_n}\tau + \frac{(4\zeta^2 - 1)}{\omega_n^2} \left\{ 1 - e^{-\zeta\omega_n\tau} \left[\cos(\omega_0\tau) + \zeta\frac{\omega_n(4\zeta^2 - 3)}{\omega_0(4\zeta^2 - 1)}\sin(\omega_0\tau) \right] \right\} \quad (35)$$

$$\bar{\delta}_{ramp} = \tau - 2\frac{\zeta}{\omega_n} + \frac{e^{-\zeta\omega_n\tau}}{\omega_n^2} \left[2\zeta\omega_n\cos(\omega_0\tau) + \frac{\zeta^2\omega_n^2 + \omega_0^2}{\omega_0}\sin(\omega_0\tau) \right] \quad (36)$$

The solutions for the overdamped case are ($\zeta > 1$):

$$\bar{\delta}_{quad} = \frac{1}{2}\tau^2 - 2\frac{\zeta}{\omega_n}\tau + \frac{(4\zeta^2 - 1)}{\omega_n^2} \left\{ 1 - e^{-\zeta\omega_n\tau} \left[\cosh(\omega_0\tau) + \zeta\frac{\omega_n(4\zeta^2 - 3)}{\omega_0(4\zeta^2 - 1)}\sinh(\omega_0\tau) \right] \right\} \quad (37)$$

$$\bar{\delta}_{ramp} = \tau - 2\frac{\zeta}{\omega_n} + \frac{e^{-\zeta\omega_n\tau}}{\omega_n^2} \left[2\zeta\omega_n\cosh(\omega_0\tau) + \frac{\zeta^2\omega_n^2 - \omega_0^2}{\omega_0}\sinh(\omega_0\tau) \right] \quad (38)$$

The solution for sawtooth waves can then be obtained combining the above results, yielding:

$$\bar{\delta}_{saw} = \sum_{n=0}^{\infty} 2\theta(\tau - n)\bar{\delta}_{quad} - \theta(\tau - n - 1)[\bar{\delta}_{step} + 2\bar{\delta}_{ramp} + 2\bar{\delta}_{quad}] \quad (39)$$

3 Results

The amplitude of the oscillatory response as a function of the dimensionless frequency and damping factor can now be assessed by making use of the relationships derived in the previous section, in order to compare the results obtained with different waveforms. For half-sinusoidal waves, the amplitude of the deformation can be calculated directly from Eq. 28 and the computed values are shown in Figures 2 and 3 for the underdamped and overdamped case, respectively. In Figure 2 it is shown that, for a given value of ζ , the amplitude reaches a maximum at a certain frequency. The locus of maxima tends to a vertical asymptote, where the amplitude becomes unbounded when $\zeta \rightarrow 0$ (or equivalently $Oh \rightarrow 0$) and $\omega_n = 2\pi$. This finding is remarkable as it is in agreement with the generally accepted criterion that incomplete coalescence is more likely when $Oh \ll 1$ (e.g. Blanchette and

Bigioni, 2006). In Figure 3, the same analysis is carried out for the overdamped system. In this case, the amplitude is always lower than the steady state deformation under constant fields, i.e. unity; it decreases with ζ and increases with the dimensionless frequency ω_n . Recalling the definition of ω_n in Eq. 15, these results show that if the electrical frequency ω_E increases, the oscillation amplitude reduces accordingly, in accord with the experimental observation of Eow and Ghadiri (2003).

The dependence of the amplitude on the model parameters for the square waves is reported in Figure 4. For overdamped systems, the behaviour is similar to that described for half-sinusoidal waves. Interestingly, when ζ becomes small, the trend of the amplitude becomes oscillatory with the presence of several maxima along the frequency axis. For $\zeta \rightarrow 0$, the amplitude tends to approach unbounded values at cyclic frequency levels, instead of a single frequency value. However, the amplitude increases faster with reducing the damping ratio at $\omega_n \approx 2\pi$ as compared to half-sinusoidal waves, which is the frequency value at which half-sinusoidal waves produce an infinite amplitude for $\zeta \rightarrow 0$. This can be seen clearly when comparing the amplitude for $\zeta=0.1$ in Figures 2 and 3. The other maxima in the amplitude versus frequency curve occur approximately at frequencies $2\pi+4\pi k$ with $k=0,1,2..$

Finally, the response obtained with sawtooth waves is described in Figure 5. The variation of the amplitude with frequency and damping ratio is similar to the previous case. However, the amplitude attains lower values at the same frequency and damping ratio. Also, the distance between consecutive amplitude peaks is shorter, as maxima are calculated at frequencies approximately equal to $2\pi+2\pi k$ with $k=0,1,2..$

4 Discussion

The results presented in the previous section reveal that the response of a conductive droplet in a dielectric oil to the electric field stimulus is strongly affected by the waveform and frequency of the field. Also, it is clearly shown that high amplitudes of oscillation can be obtained only for underdamped systems, which implies low Ohnesorge numbers (or, equivalently ζ), i.e. for large droplets. High oscillations could be beneficial for coalescence as they lead to a decrease in the stability of the interfacial film. The instability could be promoted by mechanical (undulating wave propagation over the thin film) as well as chemical means by surface tension gradients, developing due to local surfactant concentration non-uniformity caused by oscillations. The attainment of resonance has also been related to the presence of an optimum electric field frequency in terms of process efficiency (Brown and Hanson, 1965; Gong *et al.*, 2015). For underdamped systems (i.e. for large drops), the

proposed model predicts amplitudes which tend to infinite values when the Ohnesorge number tends to zero: this occurs at a single frequency level for half-sinusoidal waves and at periodic frequency values for sawtooth and square waves. However, as the droplets formed during the extraction process are relatively small (1-100 μm), the conditions for vigorous oscillations or resonance are probably hardly met. Also, the amplitude rapidly decreases with increasing applied electric field frequency; nonetheless many commercial electrocoalescers employ field frequencies in the kHz region (Mhatre *et al.*, 2015), with benefits not immediately obvious. The temporal variations of surface tension gradients, developing due to oscillations, is also unlikely to be responsive to frequencies in the kHz region. However, this topic is worthy of study to establish the most effective frequency range for this mechanism to be operative.

The trends of some literature data can now be compared with the predictions of the linear model. For this purpose, the properties of the two liquids which correspond to the sunflower oil/water system investigated by Mousavichoubeh *et al.* (2011b) are reported in Table 2. The interfacial tension has been measured as 25 mN mm^{-1} . In Figure 6, the experimental data of Eow and Ghadiri (2003) are compared with the model predictions in the form of the normalised amplitude versus electric field frequency for a 3 mm distilled water droplet in sunflower oil, using square waves voltage with 8 kV peak value. For the sunflower oil/water system, Eqs 15 and 16 give:

$$\omega_n = \frac{1.73}{\sqrt{We}} \quad (40)$$

$$\zeta = 4.23 Oh \quad (41)$$

It is evident that the difference between experiments and predictions is significant. This is probably due to small deformations approximation under which the model has been derived. However, in Figure 6, the calculated curve, obtained by modifying Eqs 40 and 41 as follows, is also reported:

$$\omega_n = \frac{1.37}{\sqrt{We}} \quad (42)$$

$$\zeta = 4.9 Oh \quad (43)$$

The agreement between experiments and predictions improves substantially by using Eqs 42 and 43, revealing that tuning of the numerical coefficients in the relationships for ω_n and ζ can effectively extend the validity of the model to systems where larger deformations occur. In Figure 7, the calculated droplet deformation is reported as a function of the electric field frequency for the square waveform. At a low frequency, namely 1 Hz, the droplet deformation follows the square field change.

However, increasing the frequency to 20 Hz leads to a significant reduction of the droplet shape oscillation. By further increasing the frequency, the oscillation amplitude becomes smaller and smaller and at 100 Hz the droplet shape remains almost stationary.

Assuming the coefficients in Eqs 42 and 43 remain the same for different waveforms and initial droplet sizes, the droplet deformation for the system studied by Mousavichoubeh *et al.* (2011b), for $R=0.492$ mm and different waveforms can now be predicted. This is shown in Figure 8. At the same value of frequency, the amplitude is the highest with square waves and the lowest with sawtooth waves. With all the waveforms, the amplitude of oscillation gradually decreases with frequency and is practically zero at 500 Hz. Also, it is interesting to observe that a value equal to half the steady-state deformation under a constant field is obtained with half-sinusoidal and square waves at 500 Hz, whereas the steady-state deformation is around 0.35 with sawtooth waves at the same frequency. The outcomes of this analysis therefore reveal notable differences in the behaviour between different waveforms in terms of the response of the oscillation amplitude to the electric field frequency. The weakening mechanism of the interfacial film due to an ever-changing droplet shape is therefore lost when the electric field frequency is too high.

The type of the applied waveform affects the electrocoalescence behaviour, as previously observed (Mhatre *et al.*, 2015). The experimental data of Mousavi *et al.* (2011b) show that the volume fraction of secondary droplets formed due to partial (incomplete) coalescence decreases as the electric field frequency is increased and the most effective waveforms are in the order: half-sinusoidal, sawtooth and square waves. The volume of secondary droplet ejected is usually the highest with square waves and the lowest with sawtooth waves. For square waves the almost total suppression of incomplete coalescence occurs at higher frequencies compared to the other two waveforms, specifically at frequencies around 50 Hz. For sawtooth waves, this threshold frequency is around 10 Hz, whereas incomplete coalescence practically disappears at 20 Hz for half-sinusoidal waves. These experimental observations are well-correlated with the results of the dynamic model of electric field induced droplet deformation developed here. The calculated amplitude of oscillation is plotted as a function of frequency and waveform in Figure 9, in which a qualitative correspondence between the experimental values of secondary volume ratio, reported by Mousavi *et al.* (2011b), and the calculated amplitude is shown. The highest amplitude is calculated with square waves, while half-sinusoidal and sawtooth waves provide a lower amplitude of oscillation. Ranking the waveforms in terms of the frequency values at which the amplitude and volume of the secondary droplet start to decrease appreciably, the same correspondence is obtained.

The qualitative agreement between experiments and theoretical analysis is notable. Further improved quantitative agreement could be obtained by tuning the coefficients of the surface tension and drag force in Eqs 42 and 43, which have some uncertainty. However, even without carrying out such an exercise, this study shows that the occurrence of incomplete coalescence is probably related to the amplitude of deformation. On the other hand, high oscillations amplitude are also most likely to promote coalescence as the interfacial film is weakened by cyclic surface deformations. The selection of the most suitable electric field parameters for the optimisation of the process efficiency therefore depends on a trade-off between enhancing the coalescence kinetics and preventing secondary droplet formation. However, the occurrence of partial coalescence it is likely to be also dependent on other factors, such as the mechanism of charge relaxation (Vivacqua *et al.*, 2016).

Conclusions

A linear dynamics model of droplet deformation due to an oscillating electric field has been developed. The dynamics of droplet deformation is described by the equation of motion of a driven damped harmonic oscillator, with the damping ratio corresponding to the Ohnesorge number and the dimensionless natural frequency depending on the Weber number. The amplitude of oscillations can increase significantly when the system is underdamped, i.e. for the Ohnesorge number tending to zero or, equivalently, for large droplets. The amplitude of shape oscillation is constant at low frequencies but it decreases rapidly at high frequencies. The model predictions are in agreement with some literature data with a slight tuning of the model parameters. The calculations based on the analytical solutions of this model show that the waveform affects the droplet dynamic response in terms of amplitude and resonance frequencies. At a given frequency, square waves generally provide higher amplitudes of oscillation, probably due to larger inertial effects associated with a rapidly varying electric field as compared to the other two waveforms. Furthermore, for half-sinusoidal waves it is possible to get resonance at a single frequency value, whilst for the other two waveforms resonance occurs cyclically when the damping factor ζ (or, equivalently the Ohnesorge number, Oh) tends to zero. The model predictions corroborate qualitatively the trend observed for the frequency dependent behaviour reported in the literature; the formation of the secondary droplets is coincident with the amplitude of oscillation of the mother droplet, with the likelihood of occurrence of partial coalescence increasing with the oscillation amplitude.

Nomenclature

a	drop interface acceleration [m/s ²]
A	dimensionless amplitude [-]
r	radial coordinate [mm]
\hat{E}	dimensionless waveform [-]
E_0	electric field strength, peak value [N·C ⁻¹]
Fr	Froude number $\rho R^2 \omega_E^2 / (\varepsilon E_0^2)$ [-]
k_E	constant in the electric field force expression [-]
Oh	Ohnesorge number $\mu / \sqrt{\rho \gamma R}$ [-]
R	drop radius [mm]
Re	Reynolds number, $\rho R^2 \omega_E / \mu$ [-]
s	Laplace domain variable [-]
We	Weber number $\rho R^3 \omega_E^2 / \gamma$ [-]
We_{el}	electrical Weber number [-]
Greek symbols	
γ	oil/water surface tension [N·m ⁻¹]
δ	dimensionless instantaneous drop deformation [-]
$\bar{\delta}$	normalized drop deformation δ / δ_{ss} [-]
δ_{ss}	steady state dimensionless drop deformation under constant field [-]
ε	oil permittivity [F·m ⁻¹]
ζ	damping ratio [-]
θ	Heaviside function [-]
λ	water/oil viscosity ratio [-]
Λ	function of the water/oil viscosity ratio [-]

μ	oil viscosity [Pa·s]
ρ	water drop density [kg m ³]
σ_γ	stress due to difference in capillary pressure [N/m ²]
$\sigma_{\gamma 0}$	stress due to difference in capillary pressure after linearisation [N/m ²]
σ_E	stress due to electrostatic pressure [N/m ²]
σ_μ	hydrodynamic stress [N/m ²]
τ	dimensionless time [-]
ω_E	electric field frequency [s ⁻¹]
ω_n	dimensionless natural frequency [-]
ω_0	dimensionless frequency defined in Eq. 22 [-]

Acknowledgements

This work was made possible by NPRP grant #5-366-2-143 from the Qatar National Research Fund (A Member of The Qatar Foundation). The statements made herein are solely the responsibility of the authors.

References

- Ajayi, O., 1978. A note on Taylor's electrohydrodynamic theory, Proc. R. Soc. Lond. A364, 499-507.
- Bailes, P.J., Larkai, S.K.L., 1981. An experimental investigation into the use of high voltage dc fields for liquid phase separation. Trans IChemE 59 (4), 229–237.
- Basaran O. A., Patzek T. W., Benner Jr R. E., Scriven L. E., 1995. Nonlinear Oscillations and Breakup of Conducting, Inviscid Drops in an Externally Applied Electric Field. Ind. Eng. Chem. Res., 34, 3454-3465.
- Baygents, J.C. and Saville, D.A., 1989. The circulation produced in a drop by an electric field: a high field strength electrokinetic model. In Drops and Bubbles: Third Int. Colloq. In Drops and Bubbles: Third Int. Colloq. (ed. T. G. Wang), pp. 7-17. American Institute of Physics.

Blanchette, F. and Bigioni, T. P 2006. Partial coalescence of drops at liquid interface. *Nature Phys.* 2, 254–257.

Brown, A.H. and Hanson, C., 1965. Effect of oscillating electric fields on coalescence in liquid–liquid systems. *Trans Faraday Soc*, 61, 1754–1760.

Davis, M.H., 1964. Two charged spherical conductors in a uniform electric field: forces and field strength. *Q. J. Mech. Appl. Math.* 17, 499–511.

Eow, J. S., and Ghadiri, M., 2003. Drop/drop coalescence in an electric field: the effects of applied electric field and electrode geometry, *Colloids and Surfaces A: Physicochem. Eng. Aspects*, 219, 253-279.

Feng, J. Q. and Scott, T. C., 1996. A computational analysis of electrohydrodynamics of a leaky dielectric drop in an electric field. *J. Fluid Mech.* 311, 289-326.

Gong, H., Peng, Y., Shang, H., Yang, Z., Zhang, X., 2015. Non-linear vibration of a water drop subjected to high-voltage pulsed electric field in oil: estimation of stretching deformation and resonance frequency. *Chem. Eng. Sci.*, 128, 21-27.

Mhatre, S., Vivacqua, V., Ghadiri, M., Abdullah, A.M., Al-Marri, M.J., Hassanpour, A., Hewakandamby, B., Azzopardi, B., Kermani B., 2015. Electrostatic phase separation: A review. *Chem Eng Res Des*, 96, 177-195.

Mousavi, S.H., Ghadiri, M. and Buckley, M., 2014. Electro-coalescence of water drops in oils under pulsatile electric fields. *Chem Eng Sci*, 120, 130 - 142.

Mousavichoubeh M., Ghadiri M. and Shariaty-Niassar M., 2011a. Electro-coalescence of an aqueous droplet at an oil–water interface, *Chem Eng Process*, 50, 338-344.

Mousavichoubeh M., Shariaty-Niassar M. and Ghadiri M., 2011b. The effect of interfacial tension on secondary drop formation in electrocoalescence of water droplets in oil, *Chem Eng Sci*, 66, 5330–5337.

Sherwood J. D., 1988. Breakup of Fluid Droplets in Electric and Magnetic Fields. *J. Fluid Mech.*, 188, 133-146.

Taylor, G. I., 1966. Studies in electrohydrodynamics. I. The circulation produced in a drop by an electric field. *Proc. R. Soc. Lond.* A291, 159-166.

Torza, S., Cox, R. G. & Mason, S. G., 1971. Electrohydrodynamic deformation and burst of liquid drops. *Phil. Trans. R. Soc. Lond.* A269, 295-319.

Vivacqua V., Mhatre S., Ghadiri M., Abdullah A. M., Hassanpour A., Al-Marri M. J., Azzopardi B., Hewakandamby B., Kermani B., 2015. Electrocoalescence of water drop trains in oil under constant and pulsatile electric fields, *Chem Eng Res Des.*, 104, 658-668.

Vivacqua V., Ghadiri M., Abdullah A. M., Hassanpour A., Al-Marri M. J., Azzopardi B., Hewakandamby B., Kermani B., 2016. Analysis of partial electrocoalescence by level-set and finite element methods. Submitted to *Chem Eng Res Des.*

Yan. H., He, L., Luo, X., Wang, J., Huang, X., Lü, Y., Yang, D., 2015. Investigation on transient oscillation of droplet deformation before conical breakup under AC electric field. *Langmuir*, 31(30), 8275-83.

Yeo L. Y., Lastochkin D., Wang S. C., Chang H. C., 2004. A New AC Electrospray Mechanism by Maxwell-Wagner Polarization and Capillary Resonance. *Phys. Rev. Lett.*, 92, 133902-1.

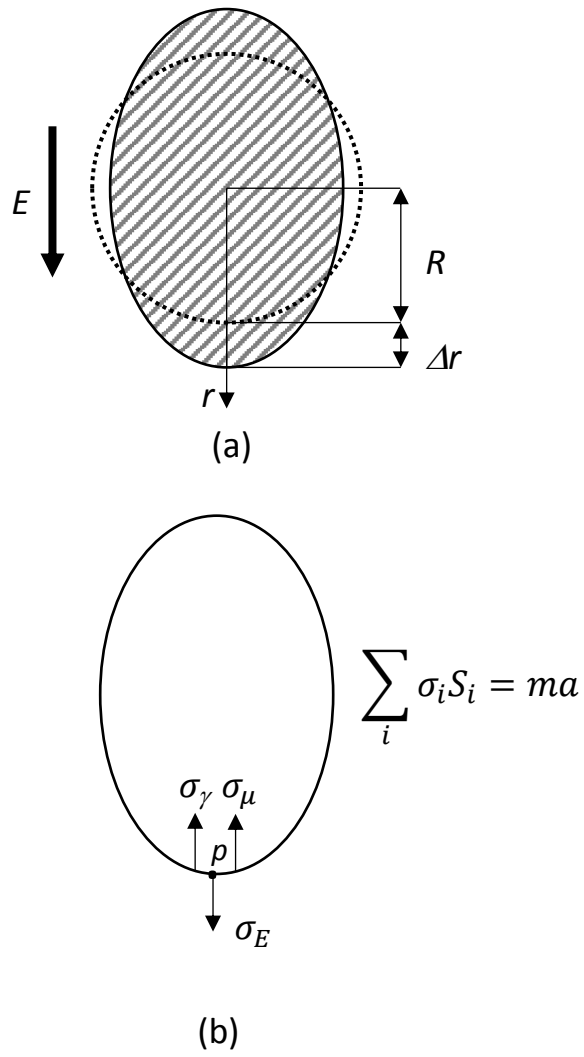


Figure 1: (a) Schematic representation of drop deformation. (b) Stresses acting on the drop.

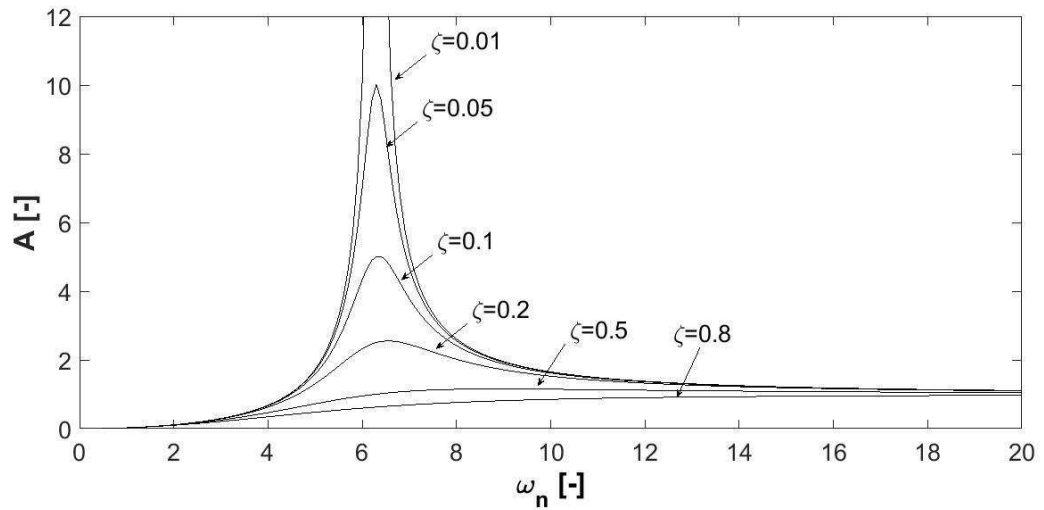


Figure 2: Amplitude of the oscillatory response as a function of the dimensionless frequency and damping factor (half-sinusoidal waves, underdamped case).

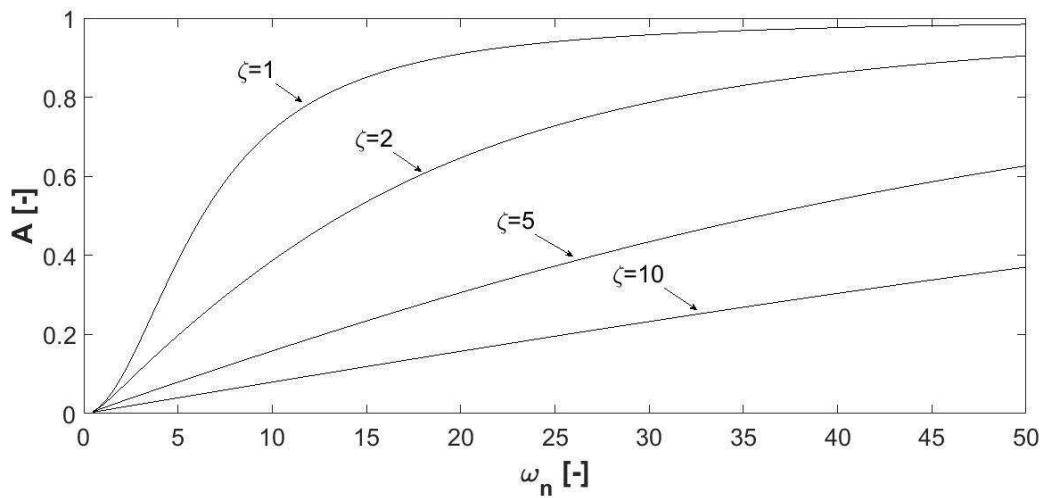


Figure 3: Amplitude of the oscillatory response as a function of the dimensionless frequency and damping factor (half-sinusoidal waves, overdamped case).

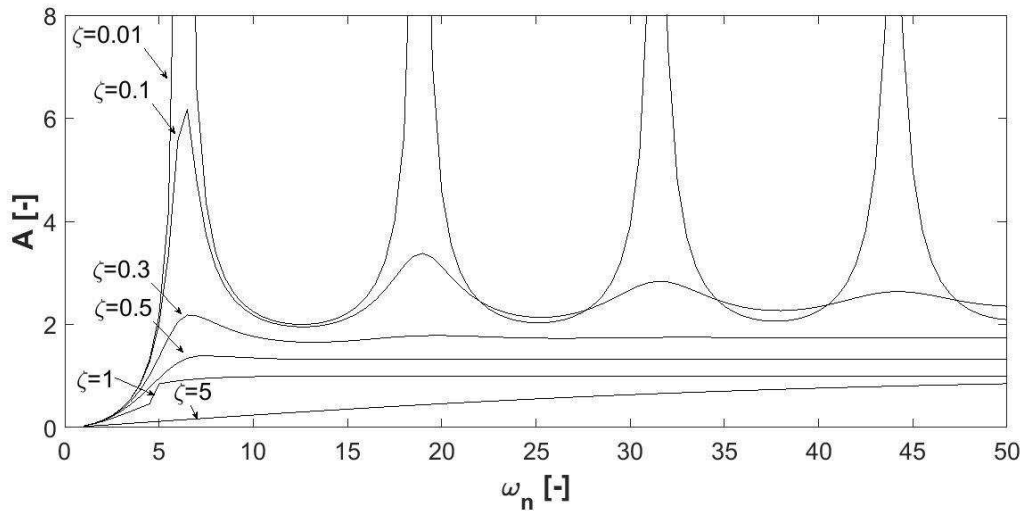


Figure 4: Amplitude of the oscillatory response as a function of the dimensionless frequency and damping factor (square waves).

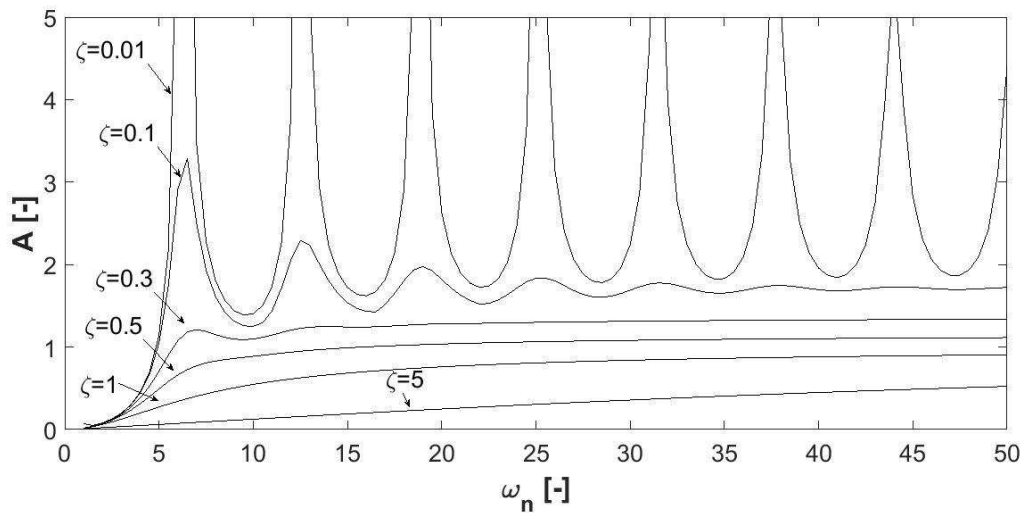


Figure 5: Amplitude of the oscillatory response as a function of the dimensionless frequency and damping factor (sawtooth waves).

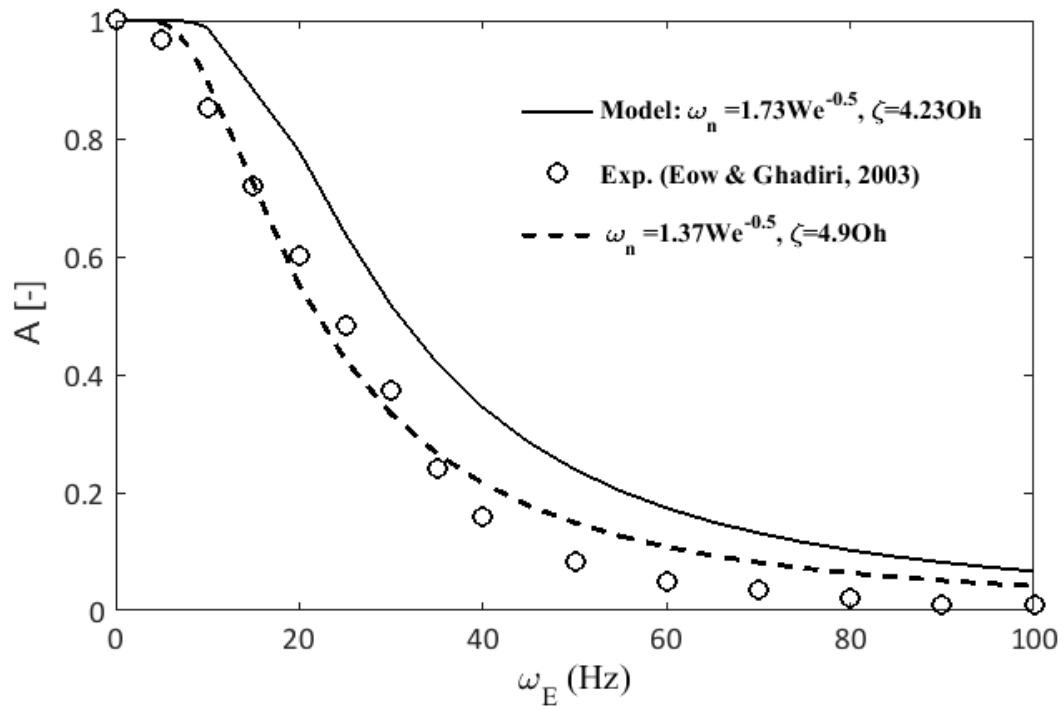


Figure 6: Comparison between model predictions and experimental values from Eow & Ghadiri (2003).

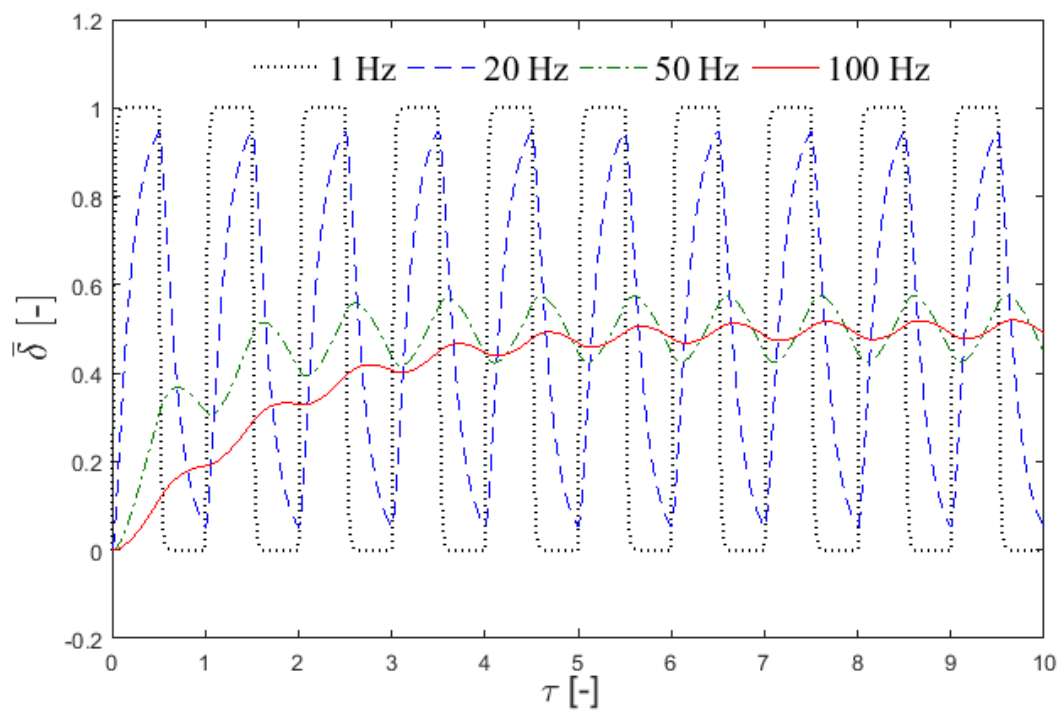
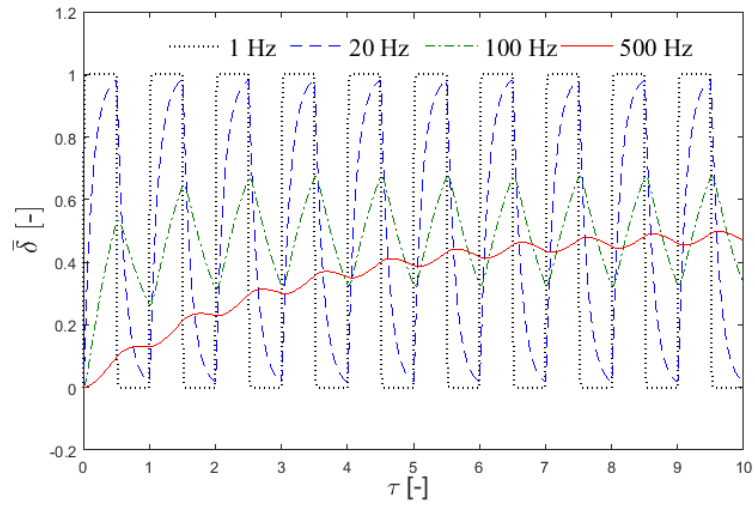
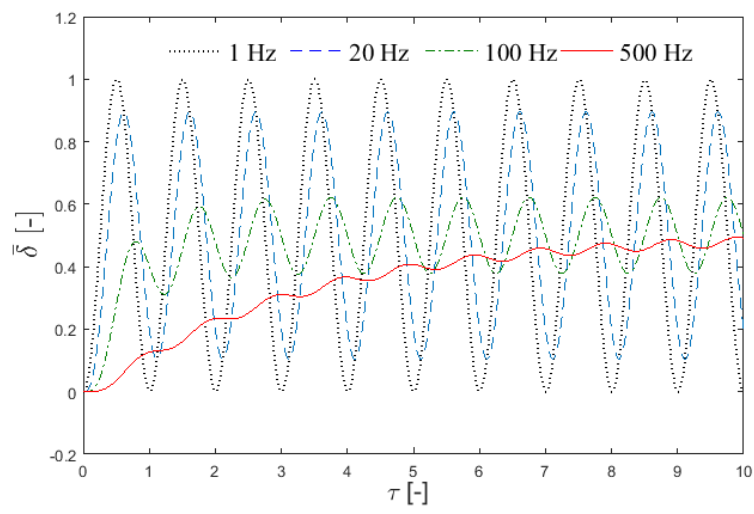


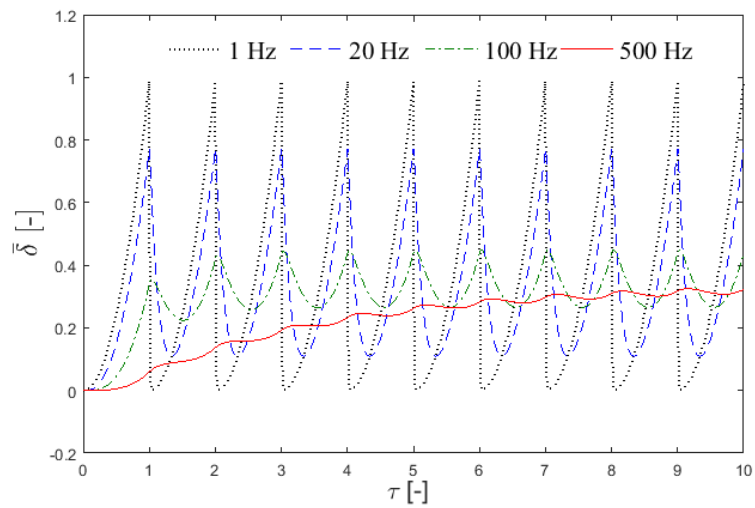
Figure 7: Predicted droplet deformation as a function of frequency for a 3 mm drop in sunflower oil under square waves.



(a)



(b)



(c)

Figure 8: Droplet deformation as a function of frequency for the system studied by Mousavichoubeh *et al.* (2011b). (a) Square waves, (b) Half-sinusoidal waves, (c) Sawtooth waves.

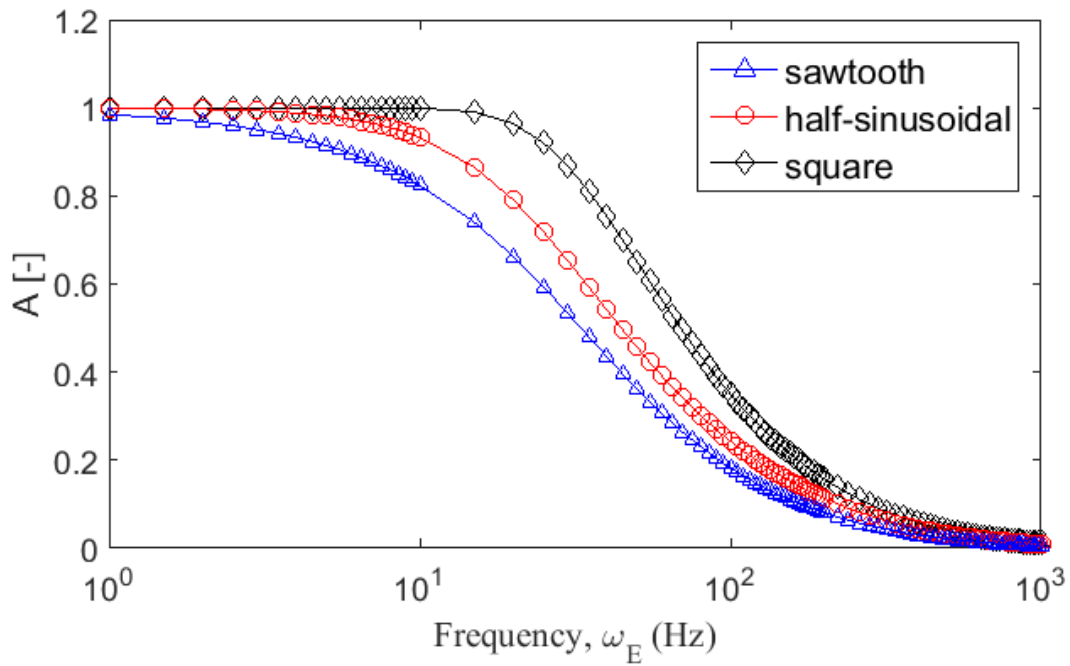


Figure 9: Amplitude of the oscillatory response as a function of frequency and waveform obtained from the dynamics model for the system investigated by Mousavi *et al.* (2014).

Table 1: Laplace transforms of the forcing functions in Eq. 18.

	Half-sinusoidal	Square	Sawtooth
$\widehat{E}_1^2(s)$	$\frac{2\pi^2}{s(s^2 + 4\pi^2)}$	$\frac{1}{s(1 + e^{-0.5s})}$	$\frac{2 - 2(s + 1)e^{-s} - s^2e^{-s}}{s^3(1 - e^{-s})}$

Table 2: Properties of the experimental liquids (after Mousavichoubeh *et al.*, 2011b).

Liquid	Conductivity $\mu\text{S m}^{-1} (\pm 5\%)$	Viscosity mPa s	Density kg m^{-3}	Dielectric constant -
Distilled water	5.49	1.00	1000	80
Sunflower oil	7.62×10^{-5}	46.5	922	4.9

